

Strong-field effects on light-induced collisional energy transfer

A. Bambini and M. Matera

Istituto di Elettronica Quantistica, Consiglio Nazionale delle Ricerche, via Panciatichi 56/30, I-50127 Firenze, Italy

A. Agresti

Dipartimento di Fisica, Sezione di Fisica Superiore, via Santa Marta 3, I-50139 Firenze, Italy

M. Bianconi

Dipartimento di Fisica, Università di Firenze, Largo Enrico Fermi 2, I-50125 Firenze, Italy

(Received 4 May 1990)

We describe strong-field effects in a class of collisional energy-transfer processes occurring among atoms in a gas irradiated by a laser beam. The time evolution of the atomic system is evaluated by solving a system of differential equations, and by using the Magnus-Light expansion of the scattering matrix. Results from the two methods are then compared. The resulting spectrum is shifted in frequency towards the antistatic side, and the line shape becomes less asymmetric. All these theoretical predictions are based on the assumption that the motion of the atoms during the collision can be described by classical mechanics, with no appreciable change of the kinetic energy of the atoms.

I. INTRODUCTION

The availability of tunable narrow-band laser sources, emitting high peak power pulses in the visible region has prompted, in the past decade, the study of laser-assisted inelastic collisions of atoms or molecules in a gas. These processes have been mainly studied in the absence of reactive channels, and follow either path

$$A_i + B_i + n\hbar\Omega \rightarrow A_f + B_f + (n-1)\hbar\Omega \quad (1.1a)$$

or

$$A_i + B_i + n\hbar\Omega \rightarrow A_f + B_f + (n+1)\hbar\Omega, \quad (1.1b)$$

depending whether the laser photon is absorbed (1.1a) or emitted (1.1b). In (1.1) A_i and B_i (A_f and B_f) denote the initial (final) states of atoms (or molecules) A and B , respectively, and Ω is the frequency of the laser field. Processes (1.1) include energy transfer,¹⁻⁵ charge transfer,⁶ or pair absorption.⁷ Studies of reactive laser-induced collisions have also been reported in the literature,⁸ demonstrating a potential interest they have for laser-assisted chemical reactions.

Laser-induced collisional energy-transfer (LICET) processes involve a second-order transition, induced by the combined collisional and radiative interactions. Unlike processes yielding collisional line broadening, in which collisions just modify the spectroscopic properties of atoms, the LICET processes can be viewed as radiative transitions of the transient molecule (quasimolecule) formed during the collision.

We are concerned here with the LICET process

$$A^* + B + \hbar\Omega \rightarrow A + B^{**} \quad (1.2)$$

where the asterisks denote excited or double excited

states of the two atoms, and the laser frequency Ω is resonant or quasiresonant with the interatomic transition frequency $\Omega_0 = [E(B^{**}) - E(A^*)]/\hbar$. This process, predicted by Gudzenko and Yakovlenko in 1972,⁹ and observed for the first time by Harris and co-workers in 1977,¹⁰ has been extensively studied both theoretically and experimentally. Transitions (1.2) are monitored by recording the fluorescence from the excited state of atom B at different laser detunings $\Delta = \Omega - \Omega_0$. The resulting spectrum, peaked at $\Delta = 0$, is strongly asymmetric, with the antistatic side falling off to zero very rapidly, and the quasistatic side extending over a wide range of laser frequencies.

In the first theoretical papers by Gudzenko and Yakovlenko⁹ and by Lisitza and Yakovlenko¹¹ the main properties of the spectrum were predicted: the width of the line core, related to the inverse of the average collision time; the cross section in the static wing, determined by the dominant R^{-6} term in the multipole expansion of the long-range interatomic potential; and the saturation properties of the peak cross section in the strong-field regime.

The first high-resolution measurements, performed by Brechignac *et al.* in 1978-80,³ revealed a discrepancy between theoretical and experimental spectral profiles in the quasistatic wing: contrary to the predicted cross-section behavior, decreasing to zero at increasing laser detunings with a constant slope of $\frac{1}{2}$, ($\sigma \sim |\Delta|^{-1/2}$), they found a different slope of 0.85. This discrepancy was explained in Refs. 12 and 13. In these papers it was shown that, in certain cases, the original description⁹ of the process, based on a two-level model, is inadequate because of the strong collisional interaction of the atoms. The refined model included a third level and yielded a wing falling off to zero with a double-slope behavior. Recent measurements,¹⁴ have shown good agreement with these

predictions, up to a laser detuning of 85 cm^{-1} .

Payne *et al.*¹⁵ have shown that a strong radiation field does affect the spectral shape in its entirety: at increasing field intensities, the spectrum becomes narrower and less asymmetric, while its peak is displaced towards the anti-static region as a consequence of the Stark dynamic shift of atomic levels. However, in this work the collisional interaction was treated to the lowest order in perturbation theory.

Results for the high-intensity field regime have also been reported by Geltman.¹⁶ In his paper, the use of a first-order perturbative treatment in the atom field coupling does not reveal the laser-induced shift of the peak frequency.

Recent measurements performed on the lithium-strontium system¹⁷ did not show any appreciable shift of the peak frequency. Moreover, the full width at half-maximum of the spectrum was found to increase at increasing laser intensities. Both these results are in contrast with theoretical predictions in Ref. 15. The only strong-field effect, predicted by existing theoretical models and experimentally observed, is the saturation effect of the resonance cross section at increasing laser intensities.

These novel difficulties in the analysis of the strong-field effects on the LICET experiment demand further investigation. The question is whether the main approximations which have been made in the theoretical models discussed so far are capable of a neat explanation of the LICET spectral profile under strong-field excitation.

We have therefore extended and fully exploited the model developed in Refs. 12 and 13 to test whether its predictions for the high-field regime fit well with experimental results. We show that, if the absence of the peak-frequency shift at high-intensity fields will be confirmed by experiments, then LICET processes in this regime do require a novel approach in which the translational degrees of freedom are included to allow for changes in the kinetic energy of colliding atoms.

In the next section we discuss the model and the main approximations on which it is based. Section III deals with the spectral profiles for the LICET process obtained by direct integration of the ensuing two- and three-level systems. In Sec. IV other methods for obtaining the total cross section for the process are discussed. Conclusions in Sec. V end the paper.

II. THE LICET PROCESS

A typical configuration of atomic energy levels in a LICET process is shown in Fig. 1. Other configurations are possible as well, as shown in Ref. 18. The transition frequencies reported in Fig. 1 are those for the europium and strontium experiment.

Compound atomic states are used throughout this paper. The states relevant to the process are

$$\begin{aligned} |1\rangle &= |\alpha\rangle|\beta^*\rangle, \\ |2\rangle &= |\alpha^*\rangle|\beta\rangle, \\ |3\rangle &= |\alpha\rangle|\beta^{**}\rangle. \end{aligned} \quad (2.1)$$

The atoms enter the LICET reaction in state $|2\rangle$, in

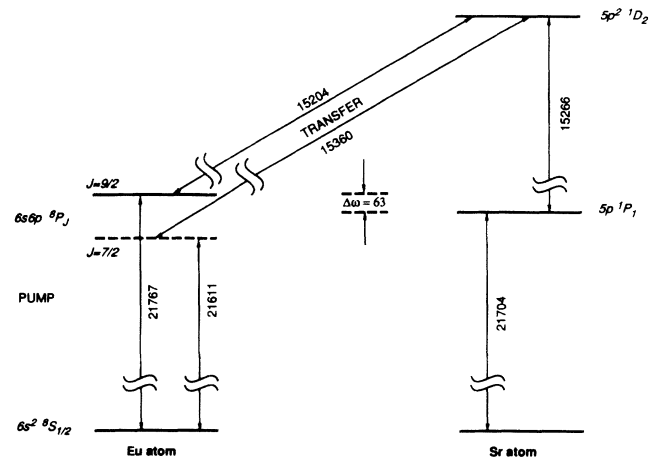


FIG. 1. The configuration of atomic energy levels of europium and strontium atoms in the LICET experiment. Transition frequencies are expressed in cm^{-1} .

which strontium is in the ground state β and europium is in the excited state α^* . During the collision, a photon from a laser field, tuned at the transition $|2\rangle \rightarrow |3\rangle$, is absorbed, and the europium excitation energy is transferred to strontium. Then the atoms leave the LICET reaction with europium in the ground state α and strontium in the double excited state β^{**} .

It should be noted that the collisional interaction between the two atoms—a dipole-dipole interaction for europium and strontium—does not couple the two states $|2\rangle$ and $|3\rangle$ directly; thus transitions between these two states would not be allowed, in the absence of a laser field, even if the energy mismatch were vanishingly small. It is the simultaneous presence of a laser field that makes the reaction possible, with the photon providing the necessary energy to grant energy conservation.

When the laser frequency is tuned at the interatomic transition frequency ω_{23} between states $|2\rangle$ and $|3\rangle$, the process is energy conserving, so that the kinetic energy of the colliding atoms remains unchanged during the collision. The situation is different, however, when the laser frequency is detuned from resonance. For the configuration shown in Fig. 1, a red detuning of the laser frequency can be compensated by the collisional shift induced on the initial state $|2\rangle$ by the state $|1\rangle$, whose energy level lies nearby. Transitions in this case occur instantaneously, when the frequency difference between the state $|2\rangle$ (displaced by the collision) and the state $|3\rangle$ (undisplaced) is matched by the laser frequency. Since this process is not energy conserving, the missing energy must be supplied by the translational degrees of freedom of the atoms: we expect the atoms to be cooled after an off-resonance transition.

By detuning the laser frequency to the opposite side, the transition probability falls to zero sharply, since no frequency matching occurs on this side of the LICET spectrum.

All these features have been found experimentally, but

they can also be drawn from a simple model that evaluates the time evolution of states (2.1) during the collision.

This model assumes the following.

(i) The colliding atoms are massive enough to prevent any change in their trajectories, due to elastic (resonant) or inelastic (off resonant) processes.

(ii) The light field is constant during the collisional interaction. This can be justified even for pulsed-laser radiation, since the collision times are much shorter than the laser pulse length.

(iii) The rotating wave approximation is used in describing the atom-field interaction.

(iv) The process involves only two colliding atoms at a time. The transition probability of the collisional event must then be averaged over all collisional parameters to get the cross section at any given laser frequency.

(v) Magnetic degeneracies of the states involved in the transition are ignored.

Under these assumptions, the internal degrees of freedom of the atoms are not coupled to the external (i.e., translational) degrees of freedom, and the quantum-mechanical amplitudes of the internal states suffice to describe the time evolution of the physical system.

The amplitudes of states (2.1) evolve with time according to

$$\begin{aligned} i\dot{\alpha}_1 &= \omega_1\alpha_1 + V\alpha_2 + \chi\alpha_3 e^{i\Omega t}, \\ i\dot{\alpha}_2 &= \omega_2\alpha_2 + V\alpha_1, \\ i\dot{\alpha}_3 &= \omega_3\alpha_3 + \chi\alpha_1 e^{-i\Omega t}, \end{aligned} \quad (2.2a)$$

or, equivalently, in the interaction picture,

$$\begin{aligned} i\dot{\alpha}_1 &= V\alpha_2 e^{i(\omega_1 - \omega_2)t} + \chi\alpha_3 e^{i(\Omega - \omega_3 + \omega_1)t}, \\ i\dot{\alpha}_2 &= V\alpha_1 e^{-i(\omega_1 - \omega_2)t}, \\ i\dot{\alpha}_3 &= \chi\alpha_1 e^{-i(\Omega - \omega_3 + \omega_1)t}. \end{aligned} \quad (2.2b)$$

In (2.2), V represents the collisional interaction potential, which, for the current case, is a dipole-dipole term of the form $V = V_0/R^3$, with

$$R = (b^2 + v^2 t^2)^{1/2}. \quad (2.3)$$

As usual, b represents the impact parameter and v the relative speed of the colliding atoms. It is apparent from (2.2) that transitions from the initial state $|2\rangle$ to the final state $|3\rangle$ occur via state $|1\rangle$: the latter state is coupled to state $|2\rangle$ by the collisional interaction, and to state $|3\rangle$ by the field.

In principle, integration of system (2.2) for a given set of collisional parameters allows us to find the probability of transition to the final state $|3\rangle$ starting from the initial condition in which state $|2\rangle$ has population 1. However, closed-form solutions of system (2.2) are not known, and one must resort to approximation schemes or numerical integration. In view of these difficulties, it is expedient to exploit all means to reduce the system to a two-level problem, which in any case will be much easier to integrate.

The substitution needed to eliminate one state would depend on the problem at hand. In a LICET process in

which the energy of state $|1\rangle$ lies far enough from the energy of state $|2\rangle$, the intermediate state will participate only virtually to the process, i.e., we expect its population to be very low at any time during the collision. Then it can be eliminated from the set in (2.2b) by means of the substitution

$$i\alpha_1 \approx \frac{V\alpha_2}{i(\omega_1 - \omega_2)} e^{i(\omega_1 - \omega_2)t} + \frac{\chi\alpha_3}{i(\Omega - \omega_3 + \omega_1)} e^{i(\Omega - \omega_3 + \omega_1)t}. \quad (2.4)$$

This approximation is justified if the highest rate of change of the amplitude of state $|1\rangle$ is provided by the exponential factors; this in turn determines the conditions under which (2.4) is valid:

$$|\omega_2 - \omega_1| \gg \left| \frac{\dot{V}}{V} \right|, \quad \left| \frac{\dot{\alpha}_2}{\alpha_2} \right|, \quad (2.5)$$

$$|\Omega - \omega_3 + \omega_1| \gg \left| \frac{\dot{\alpha}_3}{\alpha_3} \right|. \quad (2.6)$$

Moreover, the right-hand side (rhs) of Eq. (2.4) should remain small at any time, for the intermediate state to be a virtual state, which requires

$$|V| \ll |\omega_2 - \omega_1|, \quad (2.7a)$$

$$|\chi| \ll |\Omega - \omega_3 + \omega_1|. \quad (2.7b)$$

There are other situations where, although the separation of energy levels 1 and 2 (in the present configuration) is large enough for the adiabatic conditions (2.5)–(2.6) to be valid, the strength of the radiative or collisional coupling is too large to satisfy (2.7). This would certainly be the case for extremely large field strengths. But also in the low-field case, the collisional interaction may be strong enough to make (2.7a) not valid, as shown in Refs. 12 and 13. In this case we may exploit the adiabatic condition (2.5) to transform states $|1\rangle$ and $|2\rangle$ into two other states $|1'\rangle$ and $|2'\rangle$, “dressed” by the collision, among which direct transitions are unlikely to occur.

To this end, we transform the original basis of (2.2a) by the matrix \underline{T} , namely

$$\mathbf{b} = \underline{T}\mathbf{a}, \quad (2.8)$$

with

$$\underline{T} = \begin{pmatrix} \cos\theta & -\sin\theta & 0 \\ \sin\theta & \cos\theta & 0 \\ 0 & 0 & e^{i\Omega t} \end{pmatrix}. \quad (2.9)$$

The transformed vector \mathbf{b} evolves with time according to

$$i \frac{d\mathbf{b}}{dt} = \underline{T} \underline{A} \underline{T}^{-1} \mathbf{b} + i \frac{d\underline{T}}{dt} \underline{T}^{-1} \mathbf{b}, \quad (2.10)$$

where \underline{A} indicates the time-evolution matrix of the vector of quantum-mechanical amplitudes in Eq. (2.2a).

We now choose θ so that $\underline{T} \underline{A} \underline{T}^{-1}$ does not contain coupling terms among transformed states $|1'\rangle$ and $|2'\rangle$. This yields

$$\underline{T} \underline{A} \underline{T}^{-1} = \underline{D} + \underline{W}_1, \quad (2.11)$$

with

$$\underline{D} = \begin{pmatrix} \lambda_1 & 0 & 0 \\ 0 & \lambda_2 & 0 \\ 0 & 0 & \omega_3 \end{pmatrix}, \quad (2.12a)$$

$$\underline{W}_1 = \begin{pmatrix} 0 & 0 & \chi \cos\theta \\ 0 & 0 & \chi \sin\theta \\ \chi \cos\theta & \chi \sin\theta & 0 \end{pmatrix}. \quad (2.12b)$$

The eigenvalues λ_1 and λ_2 represent the instantaneous energies of the transformed states $|1'\rangle$ and $|2'\rangle$:

$$\lambda_1 = \frac{\omega_2 + \omega_1}{2} - \frac{1}{2}[(\omega_2 - \omega_1)^2 + 4V^2]^{1/2}, \quad (2.13a)$$

$$\lambda_2 = \frac{\omega_2 + \omega_1}{2} + \frac{1}{2}[(\omega_2 - \omega_1)^2 + 4V^2]^{1/2}. \quad (2.13b)$$

These eigenvalues show the repulsion of the two states during the collision. For the present configuration, λ_1 gets lower than ω_1 and λ_2 gets higher than ω_2 . As a result, their separation grows at small interatomic distances during the collision.

Nonadiabatic transitions among transformed states are induced by the term $(d\underline{T}/dt)\underline{T}^{-1}$ in (2.10). We can ignore them and set

$$\begin{aligned} \frac{d\underline{T}}{dt} &= \begin{pmatrix} -\dot{\theta} \sin\theta & -\dot{\theta} \cos\theta & 0 \\ \dot{\theta} \cos\theta & -\dot{\theta} \sin\theta & 0 \\ 0 & 0 & i\Omega e^{i\Omega t} \end{pmatrix} \\ &\approx \begin{pmatrix} 0 & 0 & 0 \\ 0 & 0 & 0 \\ 0 & 0 & i\Omega e^{i\Omega t} \end{pmatrix}, \end{aligned} \quad (2.14)$$

since $|\lambda_2 - \lambda_1| \geq |\omega_2 - \omega_1| \gg |\dot{\theta}|$, as a consequence of (2.5). Neglecting the nonadiabatic transitions does not pose any problem, as will be shown in the next section.

Under this approximation, the states $|1\rangle$ and $|2\rangle$ are dressed by the collision, and no transitions occur among them in the absence of the laser field. The latter thus couples each of these states to the final state.

This is best seen if we pass to the interaction picture to describe the time evolution of the transformed set of states. We have

$$\begin{aligned} i\dot{c}_1 &= \chi(\cos\theta)e^{i(\phi_1 - \phi_3)}c_3, \\ i\dot{c}_2 &= \chi(\sin\theta)e^{i(\phi_2 - \phi_3)}c_3, \\ i\dot{c}_3 &= \chi(\cos\theta)e^{-i(\phi_1 - \phi_3)}c_1 + \chi(\sin\theta)e^{-i(\phi_2 - \phi_3)}c_2, \end{aligned} \quad (2.15)$$

with

$$\phi_1 - \phi_3 = \int_{-\infty}^t \lambda_1 dt' - (\omega_3 - \Omega)t, \quad (2.16a)$$

$$\phi_2 - \phi_3 = \int_{-\infty}^t \lambda_2 dt' - (\omega_3 - \Omega)t. \quad (2.16b)$$

As is apparent from (2.13a), $|\lambda_1 - (\omega_3 - \omega)|$ never gets smaller than $|\omega_1 - (\omega_3 - \Omega)|$ during the collision, if the

laser frequency Ω is tuned at resonance or in the quasi-static wing of the spectrum. Thus the phase (2.16a) never gets stationary, and no crossing occurs between levels $1'$ and 3 . This allows us to perform an adiabatic elimination of state $|1\rangle$, with the same technique used to get (2.4). We require, however, that the amplitude c_1 remains much smaller than 1. This restricts the range of values of the atom-field coupling χ that can be used within this approximation:

$$|\lambda_1 - (\omega_3 - \Omega)| \gg |\chi \cos\theta|. \quad (2.17)$$

This treatment is therefore valid only for moderately strong laser fields. It should be noted that, at large in-

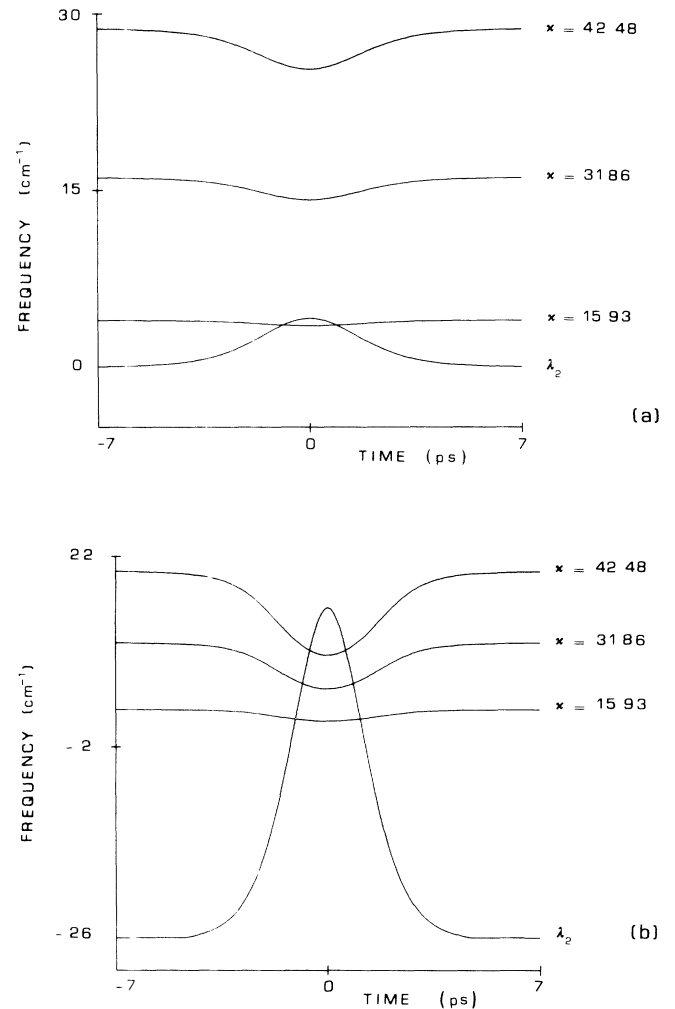


FIG. 2. The displacement of energy levels of the LICET transition during the collision. In both graphs the line labeled by λ_2 represents the eigenvalue of the dressed state $|2'\rangle$ [Eq. (2.13a)], augmented by the photon frequency Ω . The other three lines represent the shifted frequency of the final state for different field amplitudes. (a) resonance ($\Omega = \omega_3 - \omega_2$), impact parameter $b = 19$ Å. (b) quasistatic wing ($\Delta = -28$ cm $^{-1}$), $b = 12$ Å. In both figures, field amplitudes are expressed in cm $^{-1}$.

teratomic separations, condition (2.17) is the same as (2.7a).

After the elimination of state $|1\rangle$, the LICET process can be described by a simple two-state system.

$$\begin{aligned} i\dot{c}_2 &= \chi(\sin\theta)e^{i(\phi_2-\phi_3)}c_3, \\ i\dot{c}_3 &= \frac{\chi^2\cos^2\theta}{\omega_3-\Omega-\lambda_1}c_3 + \chi(\sin\theta)e^{-i(\phi_2-\phi_3)}c_2, \end{aligned} \quad (2.18)$$

while the other (intermediate) state follows adiabatically the final state

$$ic_1 \approx \frac{\chi(\cos\theta)e^{i(\phi_1-\phi_3)}}{i[\lambda_1-(\omega_3-\Omega)]}c_3. \quad (2.19)$$

The energy shift that appears in the equation for c_3 in (2.18) is a mixed Stark and collisional shift. Since for the present configuration $\omega_3-\Omega-\lambda_1$ is positive, the final level is pushed upwards, with a resulting shift of the resonance peak towards the antistatic side of the spectrum. As a consequence, the spectrum should have its maximum at laser frequencies larger than the interatomic transition frequency ω_{23} , in agreement with the results of Ref. 15. In Figs. 2(a) and 2(b) the displacement of the energy levels of states $|2'\rangle$ and $|3\rangle$ is plotted against time during the collision.

The shift depends also on the interatomic separation: since $\cos\theta$ decreases and $\lambda_1-(\omega_3-\Omega)$ increases when the two atoms come closer, level crossing becomes sharper for laser frequencies in the quasistatic wing, as shown in Fig. 2(b). This explains why the quasistatic wing is lessened in the strong-field regime and the spectrum becomes less asymmetric.

These results are confirmed by numerical integration of the system of differential equations, as shown in the next section.

III. NUMERICAL RESULTS

We have developed several FORTRAN programs to check the various stages of approximations discussed in the previous section. These programs used a Runge-Kutta-Gill method for the numerical integration of differential equations for the three- and two-state problems. Atomic transition frequencies were those for the europium and strontium configuration, shown in Fig. 1. The collisional interaction potential was the dipole-dipole potential $V=V_0/R^3$, with

$$\hbar V_0 = 2.17 \times 10^{-35} \text{ erg cm}^3. \quad (3.1)$$

All interatomic distances in the graphs to follow are expressed in units of 10^{-8}cm (\AA) and frequencies in cm^{-1} . The field amplitude is expressed in terms of the Rabi frequency related to the strontium transition β^* - β^{**} .

In Fig. 3 we show the probability of the final state of the LICET transition as a function of time. The solid lines have been obtained from the solution of the three-state problem, Eqs. (2.2b), while the dotted lines are obtained from Eqs. (2.15). In the latter equations, the terms containing $\dot{\theta}$, which are responsible for nonadiabatic

transitions between the two lower states (dressed by the collisional interaction), have been eliminated. As expected, even under strong-field excitation, the adiabatic approximation is valid. We have evaluated several graphs under different field amplitudes or frequencies, and impact parameters. In all cases, inclusion of the nonadiabatic transitions does not alter appreciably the transition probability for the LICET process.

The two-level approximation [Eqs. (2.18)], on the other hand, is not as good when the laser frequency is tuned to the blue (antistatic) side of the spectrum: for laser-field intensities large enough, the condition (2.17) for the adiabatic following of state $|1'\rangle$ [Eq. (2.19)] becomes questionable, and a correct description of the LICET process requires the inclusion of this state as a real, i.e., not virtu-

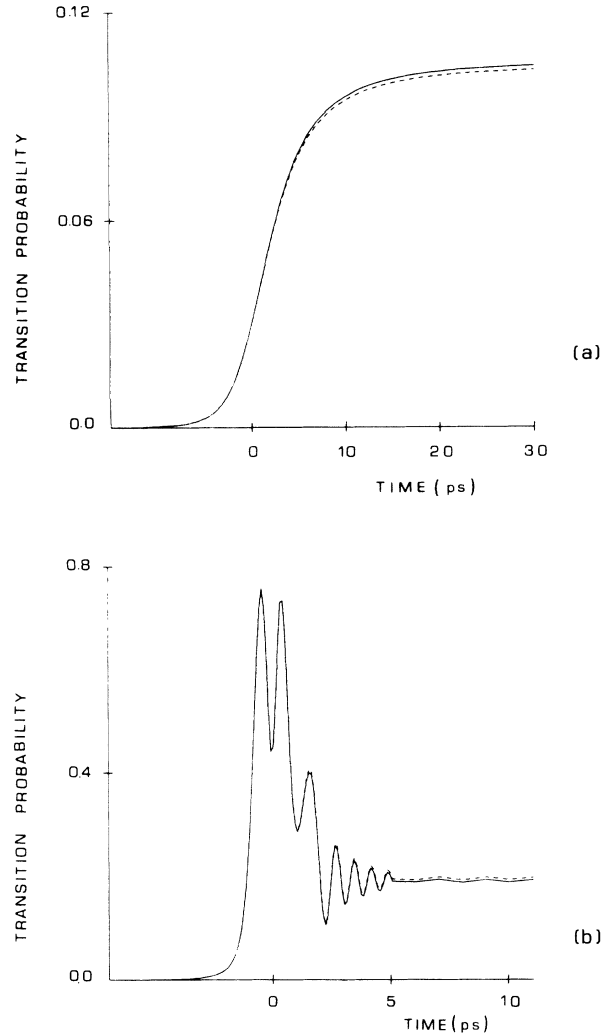


FIG. 3. Effects of nonadiabatic transitions in the LICET process. The population of the final state is plotted against time for a single collisional process. The dotted lines are obtained by neglecting nonadiabatic transitions in Eqs. (2.2b). The solid lines are obtained by integrating the full system. (a) $b=25 \text{ \AA}$, $\Delta=0$ (resonance). (b) $b=10 \text{ \AA}$, $\Delta=-55 \text{ cm}^{-1}$.

al, state. This is seen from the two graphs of Fig. 4. In the quasistatic wing, the two-level approximation [Fig. 4(a)] is acceptable, but on the opposite side [Fig. 4(b)], it yields incorrect results.

To evaluate the spectrum around its peak (which involves laser frequencies well outside the region of validity for the two-level approximation), we were therefore forced to use the three-level equations (2.15). Figure 5 shows the plot of the spectrum at its peak, for several values of the laser-field intensity. The cross section at a given laser detuning $\Delta = \Omega - (\omega_3 - \omega_2)$ and field amplitude χ was obtained by evaluating the transition probability for collisions with varying impact parameters, and then integrating over the impact parameter b ,

$$\sigma(\Delta, \chi) = 2\pi \int b P_b(\Delta, \chi) db. \quad (3.2)$$

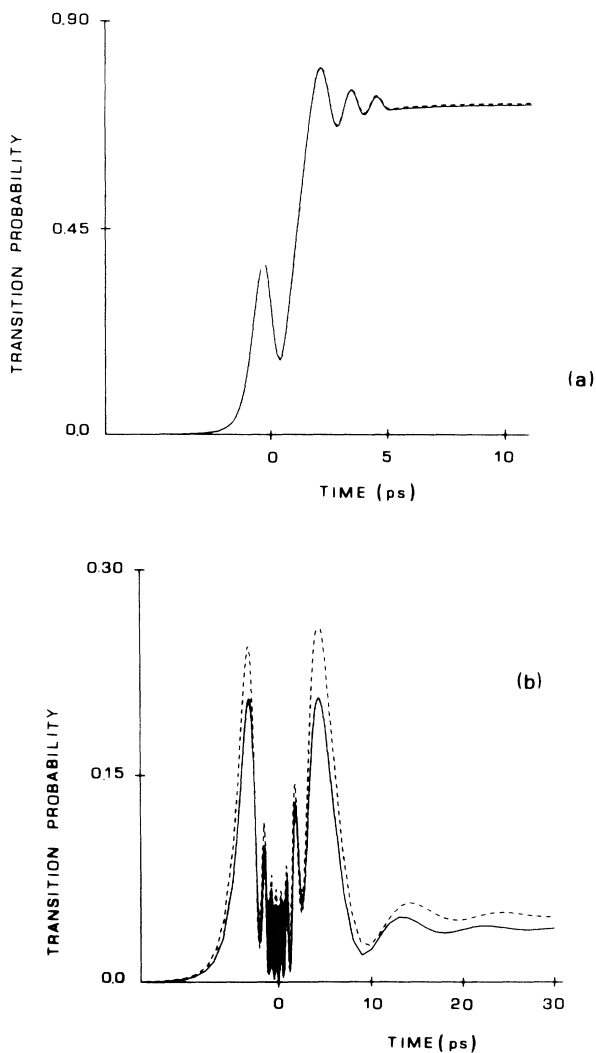


FIG. 4. Comparison of three-level (solid lines) and two-level (dotted lines) approximations. (a) quasistatic wing, $\Delta = -33 \text{ cm}^{-1}$; (b) antistatic wing, $\Delta = +8 \text{ cm}^{-1}$. In both graphs $b = 11 \text{ \AA}$.

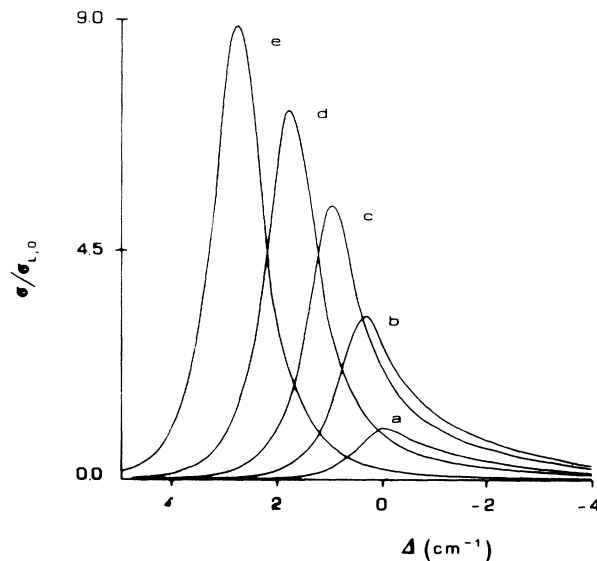


FIG. 5. The LICET spectrum near its peak for several values of the laser field intensities: (a) $\chi = 2.65 \text{ cm}^{-1}$, (b) $\chi = 5.3 \text{ cm}^{-1}$, (c) $\chi = 8 \text{ cm}^{-1}$, (d) $\chi = 10.6 \text{ cm}^{-1}$, (e) $\chi = 13.3 \text{ cm}^{-1}$.

The relative speed v was kept constant to its most likely value $6.5 \times 10^4 \text{ cm s}^{-1}$ (corresponding to a temperature of 900 K, typical of these experiments).

The shift of the peak frequency, discussed in the previous section, is apparent from Fig. 5. The figure also shows that, on the red side of the spectrum, increasing laser intensity has the effect of reducing the transition probability, as expected. The peak intensity is plotted versus the laser intensity in Fig. 6. This graph shows the

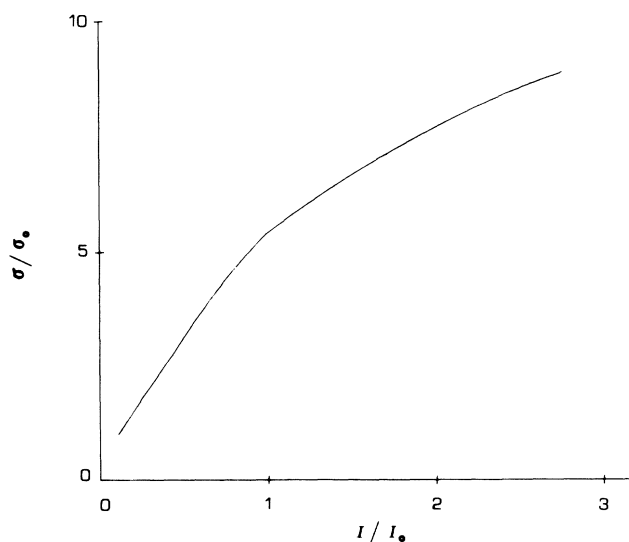


FIG. 6. The peak of the LICET spectrum plotted against the intensity of the laser field. The intensity is measured relative to the value at which saturation sets in, which in turn corresponds to a Rabi frequency of 8 cm^{-1} .

saturation effect, which sets in when the field intensity reaches a value corresponding to a Rabi frequency of 8 cm^{-1} .

The quasistatic wing of the spectrum, on the other hand, was evaluated by integrating the two-level system, Eqs. (2.18). We report in Figs. 7(a)–7(d) the wing of the spectrum for different field amplitudes. The solid line in these graphs is evaluated by minimizing the sum of quadratic deviations from the formula

$$\sigma(|\Delta|) \sim \frac{\text{const}}{|\Delta|^k (|\Delta| + \omega_2 - \omega_1)^l} \quad (3.3)$$

by using the simplex algorithm.¹⁹

The values of the parameters k and l found by this method are reported in the figure captions. We see that the double-slope behavior of the weak-field case is well reproduced in Fig. 7(a), but loses significance when the field amplitude grows.

We have also fitted the single-slope shape

$$\sigma(|\Delta|) \sim \frac{\text{const}}{|\Delta|^k}, \quad (3.4)$$

and the resulting values of k for different field amplitudes are reported in Figs. 8(a)–8(d).

As discussed in the previous section, the cross section of the LICET process does not increase linearly with the field intensity, even in the wing. Moreover, its increase is not uniform: in the near wing, the cross section grows less than in the far wing, because saturation is reached sooner. As a result, the line shape gets more and more flat at higher field intensities. The four line shapes obtained by numerical integration are collectively shown in Fig. 9 on the same scale; these effects are evident in this graph.

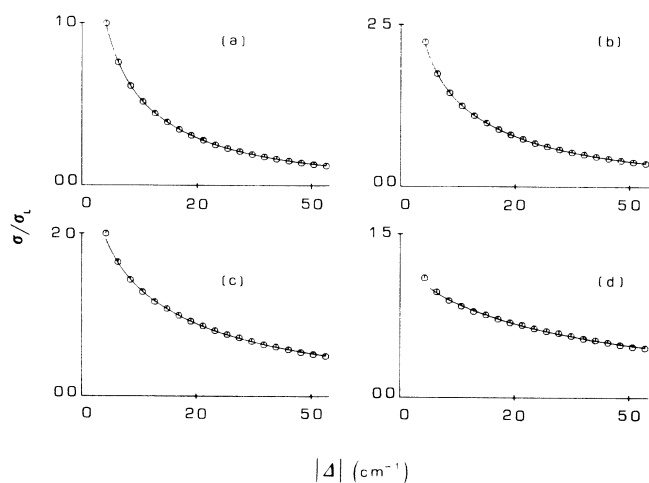


FIG. 7. The wing of the LICET spectrum fitted by the double-slope line shape [Eq. (3.3) in the text]. The values of the parameters k and l , determined by the least-square-method depend on the field amplitude. (a) $\chi = 2.65 \text{ cm}^{-1}$, $k = 0.48$, $l = 1.83$; (b) $\chi = 5.3 \text{ cm}^{-1}$, $k = 0.41$, $l = 1.59$; (c) $\chi = 8 \text{ cm}^{-1}$, $k = 0.29$, $l = 1.31$; (d) $\chi = 10.6 \text{ cm}^{-1}$, $k = 0.1$, $l = 1.11$.

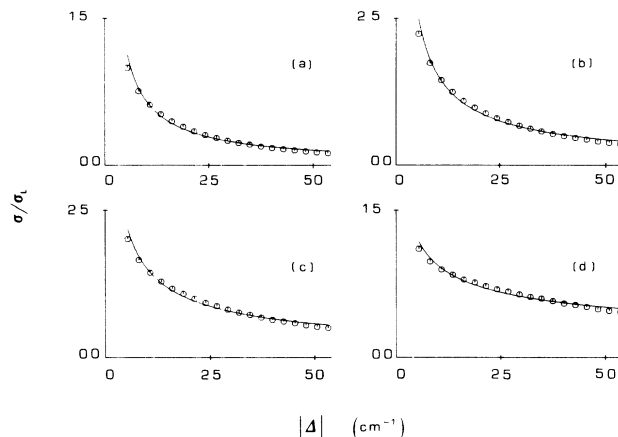


FIG. 8. The wing of the LICET spectrum fitted by the single-slope line shape [Eq. (3.4) in the text]. The field amplitudes in cases (a)–(d) are the same as in the corresponding graphs of Fig. 7. The values of k are (a) $k = 0.89$, (b) $k = 0.78$, (c) $k = 0.60$, (d) $k = 0.38$.

IV. THE MAGNUS APPROXIMATION

The numerical integration of the LICET equations can be carried out by means of standard techniques, but does not provide any physical insight into the behavior of the spectral line shape, and, for high field intensities, it is time consuming. A better alternative would be an approximation scheme to evaluate the final transition probability, to be thereafter integrated over the collisional parameters to get the cross section.

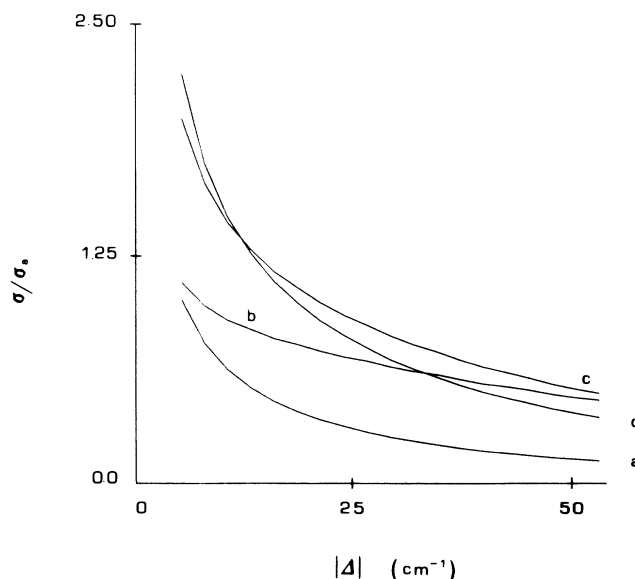


FIG. 9. The four line shapes of Figs. 7 and 8, plotted on the same scale. In the far wing, the cross section for $\chi = 13.3 \text{ cm}^{-1}$ lies below the cross section for $\chi = 10.6 \text{ cm}^{-1}$.

Standard perturbation theory is not applicable in this case, since it yields inaccurate results when evaluated to the first few orders, due to nonconservation of the total population of the compound atomic states. Attempting to evaluate the transition probability by means of the Landau-Zener formula²⁰ would not give satisfactory results, since it is known that this method may fail in cases of strong coupling.²¹ Moreover, the Landau-Zener formula applies only to transitions occurring at the level crossings, thus leaving out the region of the spectrum near its peak.

An approximate method of solution for a linear, first-order system of differential equations such as the ones of the LICET process is known under the name of Magnus-Light expansion.^{22,23} This method retains its validity in both the resonant and off-resonant cases, and has the added favorable feature of conserving the total population of states. For the system of linear equations

$$\frac{d\mathbf{x}}{dt} = \underline{A}(t)\mathbf{x}(t), \quad (4.1)$$

the Magnus-Light expansion reads²⁴

$$\mathbf{x}(t) = \exp[\underline{U}(t, -\infty)]\mathbf{x}(-\infty), \quad (4.2)$$

with

$$\underline{U}(t, -\infty) = \sum_{n=1}^{\infty} \underline{U}^n(t, -\infty), \quad (4.3)$$

$$\underline{U}^1(t, -\infty) = \int_{-\infty}^t \underline{A}(t') dt', \quad (4.4)$$

$$\underline{U}^2(t, -\infty) = \frac{1}{2} \int_{-\infty}^t dt_1 \int_{-\infty}^{t_1} dt_2 [\underline{A}(t_1), \underline{A}(t_2)]. \quad (4.5)$$

The n th term in this expansion would involve n integrals of n -fold commutators of the evolution matrix \underline{A} , evaluated at different times.

In our case, the matrix \underline{A} is of the form

$$\underline{A} = -i\underline{H}, \quad (4.6)$$

in which \underline{H} is a Hermitian matrix [see Eqs. (2.15) and (2.18)]. The first-order Magnus-Light expansion then becomes

$$\mathbf{x}(t) = \exp\left[-i \int_{-\infty}^t \underline{H}(t')\right]\mathbf{x}(-\infty), \quad (4.7)$$

which preserves the total population of the states, $\sum_i |x_i|^2$.

To evaluate transition probabilities, we must choose a state representation for which the matrix elements are integrable from $-\infty$ to $+\infty$. We need therefore to transform our equations in order to fulfill this requirement. However, this transformation is not unique. For instance, the two-level equations (2.18) could be transformed either into the system

$$i\dot{x}_2 = (\lambda_2 - \omega_2)x_2 + \chi(\sin\theta)\exp[i(\Delta - s)t]x_3, \quad (4.8)$$

$$i\dot{x}_3 = \left[\frac{\chi^2 \cos^2\theta}{\omega_3 - \Omega - \lambda_1} - s \right] x_3 + \chi(\sin\theta)\exp[i(s - \Delta)t]x_2,$$

with

$$s = \frac{\chi^2}{\omega_3 - \Omega - \omega_1}, \quad (4.9a)$$

$$\Delta = \omega_3 - \omega_2 - \Omega, \quad (4.9b)$$

or into the system

$$\begin{aligned} i\dot{x}_2 &= \chi(\sin\theta)\exp(i\psi)x_3, \\ i\dot{x}_3 &= \chi(\sin\theta)\exp(-i\psi)x_2, \end{aligned} \quad (4.10)$$

with

$$\dot{\psi} = \lambda_2 + \Omega - \omega_3 - \frac{\chi^2 \cos^2\theta}{\omega_3 - \Omega - \lambda_1}. \quad (4.11)$$

Both (4.8) and (4.10) are eligible for the Magnus-Light expansion, but they do yield quite different results. The choice of the representation must therefore be made on the basis of its aptness.

For the description of the quasistatic wing, we choose to work with (4.10). This choice is suggested by the fact that the transition probability evaluated by using the Magnus-Light expansion of (4.10) goes into first-order perturbation theory used in Refs. 12 and 13. In fact we have, using (4.7),

$$\mathbf{x}(+\infty) = \exp\left[-i\rho \begin{pmatrix} 0 & e^{i\gamma} \\ e^{-i\gamma} & 0 \end{pmatrix}\right]\mathbf{x}(-\infty), \quad (4.12)$$

with

$$\rho e^{-i\gamma} = \chi \int_{-\infty}^{+\infty} [\sin\theta(t')] \exp(-i\psi) dt'. \quad (4.13)$$

Denoting by $\underline{\Gamma}$ the matrix

$$\underline{\Gamma} = \begin{pmatrix} 0 & e^{i\gamma} \\ e^{-i\gamma} & 0 \end{pmatrix}, \quad (4.14)$$

and using the expansion

$$\begin{aligned} e^{-i\rho\underline{\Gamma}} &= \underline{1} - i\rho\underline{\Gamma} - \frac{\rho^2}{2!}\underline{1} + i\frac{\rho^3}{3!}\underline{\Gamma} + \dots \\ &= \underline{1} \cos\rho - i\underline{\Gamma} \sin\rho, \end{aligned} \quad (4.15)$$

where $\underline{1}$ represents the unit matrix, we find

$$\mathbf{x}(t) = (\cos\rho)\mathbf{x}(-\infty) - i(\sin\rho)\underline{\Gamma}\mathbf{x}(-\infty). \quad (4.16)$$

Since at $t = -\infty$ the lower state is fully populated, the vector of amplitudes is

$$\mathbf{x}(-\infty) = \begin{pmatrix} 1 \\ 0 \end{pmatrix}, \quad (4.17)$$

which, used in (4.16), yields for the probability of the final level, at $t = +\infty$, i.e., after the collision.

$$|x_3|^2 = \sin^2\rho. \quad (4.18)$$

At low values of χ , this equation becomes

$$|x_3|^2 \approx \rho^2 \approx \chi^2 \left| \int_{-\infty}^{+\infty} (\sin\theta)\exp(-i\psi) dt \right|^2, \quad (4.19)$$

with

$$\dot{\psi} \approx \lambda_2 + \Omega - \omega_3, \quad (4.20)$$

which has been used in Refs. 12 and 13 to derive the cross section of the LICET process at low laser intensities.

Equation (4.18) introduces some improvement over Eq. (4.19), but it does not cover the whole range of validity of our model, expressed by (2.17). This is shown by the graphs of Fig. 10. Carrying out the calculation for the second-order Magnus-Light approximation, we find that the final value of the amplitude vector, $\mathbf{x}(+\infty)$, is given by

$$\mathbf{x}(+\infty) = \exp[-i(\rho\mathbf{\Gamma} + \nu\hat{\sigma}_z)]\mathbf{x}(-\infty), \quad (4.21)$$

where $\hat{\sigma}_z$ is the \hat{z} component of the Pauli spin vector operator, and ν is given by

$$\nu = 2\chi^2 \int_{-\infty}^{+\infty} dt_2 \int_{-\infty}^{t_2} dt_1 \sin[\theta(t_1)] \sin[\theta(t_2)] \times \sin[\psi(t_2) - \psi(t_1)]. \quad (4.22)$$

Since the exponent in (4.21) can be expressed in terms of the scalar product

$$\rho\mathbf{\Gamma} + \nu\hat{\sigma}_1 = \mathbf{R} \cdot \boldsymbol{\sigma}, \quad (4.23)$$

with

$$\mathbf{R} = (\rho \cos\gamma, \rho \sin\gamma, \nu), \quad (4.24)$$

we find, using an expansion similar to (4.15),

$$\begin{aligned} \exp(-i\mathbf{R} \cdot \boldsymbol{\sigma}) &= \cos|R| - i \frac{\mathbf{R} \cdot \boldsymbol{\sigma}}{|R|} \sin|R| \\ &= \begin{pmatrix} \cos|R| - i \frac{R_z}{|R|} \sin|R| & \left[-i \frac{R_x}{|R|} + \frac{R_y}{|R|} \right] \sin|R| \\ \left[-i \frac{R_x}{|R|} - \frac{R_y}{|R|} \right] \sin|R| & \cos|R| + i \frac{R_z}{|R|} \sin|R| \end{pmatrix}, \end{aligned} \quad (4.25)$$

which leads to the transition probability

$$|x_3| = \rho^2 \frac{\sin^2(\rho^2 + \nu^2)^{1/2}}{\rho^2 + \nu^2}. \quad (4.26)$$

Equation (4.26) introduces a slight improvement over Eq. (4.18), but still we cannot cover the whole range of validity of our model. Use of higher-order terms would be prohibitive, however, since the calculation of multiple integrals becomes soon more lengthy than the numerical integration of the original Eqs. (4.10).

To evaluate transition probabilities in the core of the spectral line shape it is expedient to start the Magnus-Light expansion from Eqs. (4.8). Setting

$$\delta_2 = \lambda_2 - \omega_2, \quad (4.27a)$$

$$\delta_3 = \frac{\chi^2 \cos^2\theta}{\omega_3 - \Omega - \lambda_1} - s, \quad (4.27b)$$

and

$$W(t) = \chi(\sin\theta) \exp[i(\Delta - s)t], \quad (4.28)$$

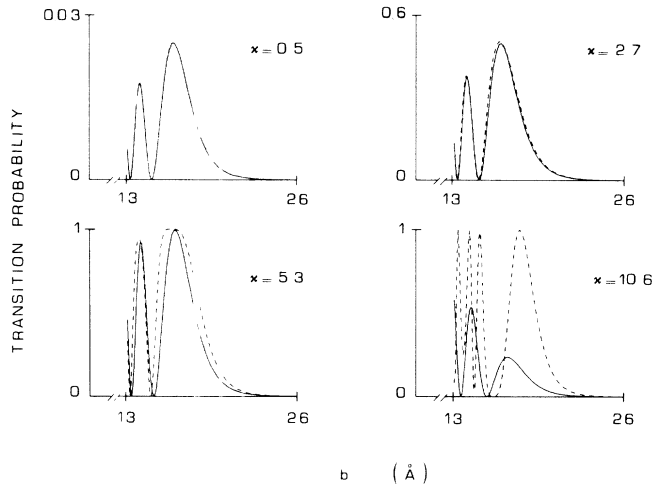


FIG. 10. Comparison between the first-order Magnus-Light approximation (dotted lines) and numerical integration (solid lines) in the two-level approximation. The graphs show the transition probability vs the impact parameter, with $\Delta = 10.6 \text{ cm}^{-1}$ for all graphs. The two methods give the same results for field amplitudes up to 5 cm^{-1} .

we find, to the lowest-order approximation,

$$\mathbf{x}(+\infty) = \exp \left[-i \int_{-\infty}^{+\infty} \begin{pmatrix} \delta_2 & W \\ W^* & \delta_3 \end{pmatrix} dt \right] \mathbf{x}(-\infty). \quad (4.29)$$

Using the expansion (4.25), this equation yields for the transition probability the expression

$$|x_3|^2 = \frac{\alpha^2 + \beta^2}{\alpha^2 + \beta^2 + \eta^2} \sin^2 S, \quad (4.30)$$

where

$$\alpha - i\beta = \int W(t') dt', \quad (4.31)$$

$$\eta = \frac{1}{2} \int (\delta_2 - \delta_3) dt', \quad (4.32)$$

and

$$S = (\alpha^2 + \beta^2 + \eta^2)^{1/2}. \quad (4.33)$$

It should be noted that, as stated earlier, Eq. (4.30) provides a different transition probability than Eq. (4.18).

For instance, Eq. (4.30) does not allow for a total transfer of population from the lower to the upper state (for which we would have $|x_3|^2=1$), while Eq. (4.18) does.

The choice of the representation (4.8) leads to a formula for the transition probability that can be readily interpreted: the transition probability depends on $\alpha^2+\beta^2$, which is the square modulus of the Fourier transform of $\chi \sin\theta$ evaluated at $\Delta-s$. This in turn is the effective detuning of the laser field from the LICET transition at large interatomic distances. This formula is therefore appropriate for cases in which no level crossing occurs, i.e., at (or near) resonance. On the contrary, Eq. (4.18) contains the integral of $\sin\theta \exp(-i\psi)$ which is rapidly oscillating everywhere, except at those points in which the phase ψ is stationary. Thus, Eq. (4.18) is more appropriate for evaluating transition probabilities in spectral regions where leading terms come from level crossing.

Formula (4.30) can be even evaluated analytically for the case of exact resonance $\Delta=s$ (when the shift s of the final level is compensated by the laser detuning Δ), and for large impact parameters b , for which the collisional interaction V is small enough compared to $|\omega_2-\omega_1|$. We find

$$\eta \approx \frac{1}{2} \int \delta_2 dt' = \frac{3}{16} \pi \frac{V_0^2}{|\omega_2-\omega_1|} \frac{1}{vb^5} \quad (4.34)$$

and

$$\alpha \approx \int_{-\infty}^{+\infty} \frac{\chi V dt'}{|\omega_2-\omega_1|} = \frac{2\chi V_0}{|\omega_2-\omega_1|} \frac{1}{vb^2}, \quad (4.35a)$$

$$\beta \approx 0. \quad (4.35b)$$

Averaging over the impact parameter b requires a single integration to get the cross section at the resonance peak.

The two-level approximation, however, is slightly inaccurate near the central region of the spectrum, particularly in the antistatic side of the line shape, and the three-level approximation may be needed in some instances. The Magnus-Light expansion can be carried out for the three-level case, too, although we lose the simplicity brought in by the use of the Pauli σ spin matrices. We give here a few hints on how to evaluate the Magnus-Light expansion in this case.

Equations (2.15) or their counterparts in the Schrödinger representation are not suitable for this purpose, since the matrix element that couples state $|1'\rangle$ to state $|3\rangle$ does not vanish at $t=\pm\infty$, due to our assumption of a constant field amplitude χ .

We rewrite Eqs. (2.10), omitting the $\dot{\theta}$ terms, in the form

$$i \frac{d\mathbf{b}}{dt} = (\underline{B}_0 + \underline{B}_c) \mathbf{b}, \quad (4.36)$$

with

$$\underline{B}_0 = \begin{pmatrix} \omega_1 & 0 & \chi \\ 0 & \omega_2 & 0 \\ \chi & 0 & \omega_3 - \Omega \end{pmatrix}, \quad (4.37a)$$

$$\underline{B}_c = \begin{pmatrix} \lambda_1 - \omega_1 & 0 & \chi(\cos\theta - 1) \\ 0 & \lambda_2 - \omega_2 & \chi \sin\theta \\ \chi(\cos\theta - 1) & \chi \sin\theta & 0 \end{pmatrix}, \quad (4.37b)$$

and we transform \mathbf{b} by means of

$$\mathbf{d} = \underline{U} \mathbf{b}, \quad (4.38)$$

choosing the transformation matrix \underline{U} such that

$$\underline{U} \underline{B}_0 \underline{U}^{-1} = \underline{F}_0, \quad (4.39)$$

with \underline{F}_0 diagonal. The transformation matrix \underline{U} has the form

$$\underline{U} = \begin{pmatrix} \cos\xi & 0 & \sin\xi \\ 0 & 1 & 0 \\ -\sin\xi & 0 & \cos\xi \end{pmatrix}, \quad (4.40)$$

with ξ constant. It should be noted that \underline{B}_c and its transform $\underline{F}_c = \underline{U} \underline{B}_c \underline{U}^{-1}$ vanish at $t \pm \infty$, as required.

The vector \mathbf{d} then evolves with time according to

$$i \frac{d\mathbf{d}}{dt} = \underline{F}_0 \mathbf{d} + \underline{F}_c \mathbf{d}. \quad (4.41)$$

By means of further transformations, we may either pass to the interaction picture, in which the diagonal terms are missing, or make the diagonal terms vanishing just at $t = \pm\infty$, in a form that parallels Eqs. (4.8) for the two-level problem. In the first case, we have to remove the diagonal terms in both \underline{F}_0 and \underline{F}_c , while in the second case we have to remove just the constant parts of the diagonal terms in \underline{F}_0 . Here, again, we have the ambiguity in the choice of the equations to use, as discussed above.

We show here the final result for the second case only. The vector \mathbf{d} at $t = +\infty$ is expressed in terms of the vector \mathbf{d} at $t = -\infty$ by the relation

$$\mathbf{d}(+\infty) = \underline{Y}^{-1} \exp \left[-i \int_{-\infty}^{+\infty} \underline{G}(t) dt \right] \underline{Y} \mathbf{d}(-\infty), \quad (4.42)$$

in which we have set

$$\underline{Y} = \begin{pmatrix} e^{i\mu_1 t} & 0 & 0 \\ 0 & e^{i\mu_2 t} & 0 \\ 0 & 0 & e^{i\mu_3 t} \end{pmatrix}, \quad (4.43)$$

with

$$\mu_1 = \frac{\omega_1 + \omega_3 - \Omega}{2} - \left[\left[\frac{\omega_1 + \omega_3 - \Omega}{2} \right]^2 - \omega_1(\omega_3 - \Omega) + \chi^2 \right]^{1/2}, \quad (4.44a)$$

$$\mu_2 = \omega_2, \quad (4.44b)$$

$$\mu_3 = \frac{\omega_1 + \omega_3 - \Omega}{2} + \left[\left[\frac{\omega_1 + \omega_3 - \Omega}{2} \right]^2 - \omega_1(\omega_3 - \Omega) + \chi^2 \right]^{1/2}, \quad (4.44c)$$

and the matrix \underline{G} given by

$$\begin{aligned}
G_{11} &= h_1 \cos^2 \xi - k \sin 2\xi, \\
G_{12} &= -l \sin \xi e^{i(\mu_1 - \mu_2)t}, \\
G_{13} &= (h_1 \sin \xi \cos \xi + k \cos 2\xi) e^{i(\mu_1 - \mu_3)t}, \\
G_{22} &= h_2, \\
G_{23} &= l \cos \xi e^{i(\mu_2 - \mu_3)t}, \\
G_{33} &= h_1 \sin^2 \xi + k \sin 2\xi, \\
G_{jk} &= G_{kl}^*,
\end{aligned} \tag{4.45}$$

with

$$\begin{aligned}
\tan \xi &= \frac{\omega_1 - \mu_1}{\chi}, \\
h_1 &= \lambda_1 - \omega_1, \\
h_2 &= \lambda_2 - \omega_2, \\
k &= \chi(\cos \theta - 1), \\
l &= \chi \sin \theta.
\end{aligned} \tag{4.46}$$

It should be noted that the initial conditions for \mathbf{d} are the same as those for \mathbf{b} , if the LICET process starts with state $|2\rangle$ populated (direct LICET process), but, for the inverse LICET process in which state $|3\rangle$ is initially populated, they are different.

The first-order Magnus-Light expansion for the three-level process involves three or five integrations of rapidly oscillating functions and the numerical process of diagonalizing a 3×3 Hermitian matrix, but still calculations are faster than the numerical integration of the original system. The second-order expansion, which involves double integrations, is prohibitively longer and does not provide, as for the case of the two-level system, any great

improvement over the first-order expansion.

In this work, we have tested all the formulas given in this section and compared the results with those obtained by numerical integrations. In Fig. 11 we show the plots of the transition probabilities versus the impact parameter b for several cases. As with the two-level problem, the three-level Magnus expansion provides some improvement over first-order perturbation theory, but becomes soon unreliable for laser field amplitudes of the order of 8 cm^{-1} .

V. CONCLUSIONS

In this paper we have extended the model developed in Refs. 12 and 13 to treat the effects of high-intensity laser fields on the LICET spectrum. We have also discussed several approximation formulas, based on the Magnus-Light expansion, that may prove useful in obtaining directly the cross section of the process, avoiding the numerical integration of the two- or three-state systems of differential equations.

The results discussed in this paper show that, in contrast with experimental findings, the LICET spectrum is shifted in frequency, as an effect of the strong laser field, towards the antistatic side. Moreover, the spectral line shape tends to lose asymmetry, because the cross section in the quasistatic wing is lowered by the presence of a combined light and collisional shift that reduces the effective time for level crossing. At high fields, the wing of the quasistatic region loses the double-slope feature that characterizes the low-field regime, and tends to become more flat. The average slope passes from 0.85 at low fields to 0.4 at high fields.

These results confirm that theoretical predictions, based on the assumptions described in Sec. II, are in conflict with existing experimental results.¹⁷ If the latter will be confirmed, then the assumptions that are usually done in the theoretical description of these processes must be scrutinized with care. We outline here the possible weaknesses of the model.

(i) The interatomic, collisional potential does not affect the atomic motion: the atoms do not deviate from a straight trajectory and move with a constant velocity. This assumption notably simplifies the treatment. But if it fails, then we must consider that the interatomic potential does depend on the state in which the system is, in view of the appreciable population the upper state gets during the interaction. Thus, atomic trajectories cannot be considered as classical trajectories any longer.

(ii) Magnetic degeneracies may play a role in the process as well. Each magnetic sublevel has its own energy shift during the collision, and frequency matching occurs on a wider time interval, thus affecting the transition cross section.

(iii) For close collisions, the spin-orbit energy splitting in the europium atoms is of the same order as the collisional potential. Thus, the $J = \frac{7}{2}$ and $\frac{5}{2}$ states of the europium might be involved in the transition process.

The achievement of an acceptable agreement between theoretical and experimental results in this field is not only an academic exercise. Because of their inherent

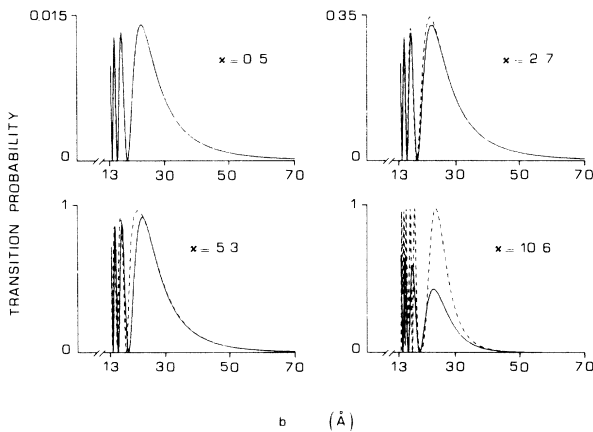


FIG. 11. Comparison between the first-order Magnus-Light approximation (dotted lines) and numerical integration (solid lines) in the three-level approximation. The graphs show the transition probability vs the impact parameter, with $\Delta = 0$. Here, too, the two methods give diverging results as the field amplitude grows over 5 cm^{-1} .

feature of tunability, and the possibility of controlling the process via laser intensities, the LICET processes (or other, related processes) might play a role as a tool for cooling colliding atoms confined in a trap. The mechanism is much more efficient than optical cooling obtained by means of quasioresonant laser beams, since for each collisional event followed by the absorption of a photon, we

can subtract an energy as large as $5\text{--}10\text{ cm}^{-1}$, contrasted to an energy of $\hbar k p / m \approx 3 \times 10^{-2}\text{ cm}^{-1}$ that can be subtracted in each elementary process via optical cooling. Selective cooling of the translational degrees of freedom, on the other hand, might prove an efficient mechanism for the enhancement of molecular reactions in the presence of a laser field.

-
- ¹A. Gallagher and T. Holstein, *Phys. Rev. A* **16**, 2413 (1977).
²S. Yeh and P. R. Berman, *Phys. Rev. A* **19**, 1106 (1979).
³C. Brechignac, Ph. Cahuzac, and P. E. Toschek, *Phys. Rev. A* **21**, 1969 (1980).
⁴P. Hering and Y. Rabin, *Chem. Phys. Lett.* **77**, 506 (1981).
⁵J. Lukasik and S. C. Wallace, *Phys. Rev. Lett.* **47**, 240 (1981).
⁶W. R. Green, M. D. Wright, J. F. Young, and S. E. Harris, *Phys. Rev. Lett.* **43**, 120 (1979).
⁷J. C. White, G. A. Zdasiuk, J. F. Young, and S. E. Harris, *Opt. Lett.* **4**, 137 (1979).
⁸P. D. Kleiber, A. M. Lyyra, K. M. Sando, V. Zarfirooulos, and W. C. Stwalley, *J. Chem. Phys.* **85**, 5493 (1986).
⁹L. I. Gudzenko and S. I. Yakovlenko, *Zh. Eksp. Teor. Fiz.* **62**, 1686 (1972) [*Sov. Phys.—JETP* **35**, 877 (1977)].
¹⁰R. W. Falcone, W. R. Green, J. C. White, J. F. Young, and S. E. Harris, *Phys. Rev. A* **15**, 1333 (1977).
¹¹V. S. Lisitsa and S. I. Yakovlenko, *Zh. Eksp. Teor. Fiz.* **66**, 1550 (1974) [*Sov. Phys.—JETP* **39**, 759 (1974)].
¹²A. Bambini and P. R. Berman, in *Photons and Continuum States of Atoms and Molecules*, edited by N. K. Rahman, C. Guidotti, and M. Allegrini (Springer-Verlag, Berlin, 1987), p. 220–226; *Phys. Rev. A* **35**, 3753 (1987).
¹³A. Agresti, P. R. Berman, A. Bambini, and A. Stefanel, *Phys. Rev. A* **38**, 2259 (1988).
¹⁴M. Matera, M. Bianconi, R. Buffa, L. Fini, and M. Mazzoni, *Phys. Rev. A* **41**, 3766 (1990).
¹⁵M. G. Payne, V. E. Anderson, and J. E. Turner, *Phys. Rev. A* **20**, 1032 (1979).
¹⁶S. Geltman, *Phys. Rev. A* **35**, 3775 (1987).
¹⁷F. Dorsch, S. Geltman, and P. E. Toschek, *Phys. Rev. A* **37**, 2441 (1988).
¹⁸P. R. Berman, *Phys. Rev. A* **22**, 1838 (1980).
¹⁹J. A. Nelder and R. Mead, *Comput. J.* **7**, 308 (1965).
²⁰L. Landau, *J. Phys. Moscow* **2**, 46 (1932); C. Zener, *Proc. R. Soc. London Ser. A* **137**, 696 (1933).
²¹J. Light and A. Szoke, *Phys. Rev. A* **18**, 1363 (1978).
²²J. C. Light, *J. Chem. Phys.* **66**, 5241 (1977).
²³P. A. Rodgers and S. Swain, *J. Phys. B* **20**, 617 (1987).
²⁴P. Pechukas and J. C. Light, *J. Chem. Phys.* **44**, 3897 (1966).